Satellite remote sensing of submesoscale fronts in inner seas

Marina I. Mityagina, Olga Yu. Lavrova

Marina I. Mityagina, Olga Yu. Lavrova, "Satellite remote sensing of submesoscale fronts in inner seas," Proc. SPIE 10784, Remote Sensing of the Ocean, Sea Ice, Coastal Waters, and Large Water Regions 2018, 107840Y (10 October 2018); doi: 10.1117/12.2323974

SPIE.

Event: SPIE Remote Sensing, 2018, Berlin, Germany

Satellite Remote Sensing of Submesoscale Fronts in Inner Seas

Marina I. Mityagina and Olga Yu. Lavrova
Space Research Institute, Russian Academy of Sciences,
117997, Moscow, Russia, Profsoyuznaya str. 84/32

ABSTRACT

The work studies submesoscale fronts (with characteristic transverse scales lower than the Rossby internal radius of deformation) in inland seas on the base of remote sensing data. We show that we can significantly broaden our insights into the physics and geography of small-scale fronts by employing satellite synthetic aperture radar (SAR). During our satellite survey of the Baltic Sea, we obtained many satellite images of the sea surface bearing imprints of fronts of different formation mechanisms and different spatial and temporal characteristics. First we develop a methodology for identifying various submesoscale front signatures in SAR images and list the most common features of front manifestations. We describe characteristic features associated with fronts of different nature which are not usually detectable by traditional observational data sources because of their small scale and because they are often masked by upper-level clouds. The main problem is to discriminate between signatures of fronts in the sea and those in the near-surface layer of the atmosphere. We validated our interpretations of front features in SAR images via the combined analysis of data on the sea surface and marine atmosphere condition, sea surface temperature, and mesoscale water dynamics.

Keywords: satellite remote sensing, sea surface, satellite SAR, atmospheric fronts, river plums, hydrological fronts, thermal fronts, the Baltic Sea

INTRODUCTION

Fronts and frontal zones represent one of the essential elements of water dynamics, namely the natural boundaries between waters with different thermodynamic parameters. They are notable for having a complex structure and a high spatial-temporal variability. Fronts in the ocean or in the atmosphere are the zones where properties of air or water masses change sufficiently at a relatively short distance. This distance depends on the scale of the process responsible for the existence of the front. Depending on their scale, fronts can be divided into large-scale climate-related fronts (planetary) created by continually acting climatic factors, mesoscale fronts associated with synoptic-scale processes in the ocean, and small-scale fronts of local origin[1]. Fronts play a vital role in the energy transfer along a cascade of scales from global circulation (thousands of kilometers) to small-scale phenomena (meters)[2]. The width of fronts in the deep ocean reaches 100 km, while estuarine fronts can be only a few meters wide. Regardless of their size, fronts can by defined as the zones where the horizontal gradient of one or several characteristics (temperature, salinity, density, velocity, etc.) reaches its maximum.

Remote sensing methods of studying the ocean are especially useful in investigations of fronts in the ocean and in the marine atmosphere. Great attention is given to studying these phenomena by scientists worldwide. The rapid development of these studies has been greatly stimulated by the improvement of satellite remote sensing methods in the infra-red (IR) and visible (VIS) ranges of the electromagnetic spectrum. However, to the present day, mostly large-scale oceanic fronts in climatic and synoptic frontal zones remain the subject of numerous experimental and theoretical studies[3, 4]. Some recent studies described large-scale oceanic fronts associated with major currents[4, 5, 6]. Other publications studied fronts near Alaska[7, 8, 9], near the Iberian Peninsula[10, 11], on the continental shelf off the northeast U.S. coast[12], and in the Baltic Sea[13]. Some studies were able to correlate occurrences of fronts with atmospheric or oceanic forcing sources[14].

Meantime, the research on submesoscale fronts (with characteristic transverse scales lower than the Rossby internal radius of deformation) in closed seas is scarce. These phenomena are too complex to be studied by traditional methods due to their non-stationarity, spontaneity of their appearance and their relatively short lifetime.

For more than two decades, the monitoring of frontal zones and fronts in the ocean has been performed using optical satellite remote sensing. A significant limitation for observing the sea surface from space in the optical range is the

Remote Sensing of the Ocean, Sea Ice, Coastal Waters, and Large Water Regions 2018,
edited by Charles R. Bostater, Stelios P. Mertikas, Xavier Neyt, Proc. of SPIE Vol. 10784,
107840Y · © 2018 SPIE · CCC code: 0277-786X/18/$18 · doi: 10.1117/12.2323974

presence of clouds and insufficient illumination. The Synthetic Aperture Radar (SAR) is a very informative tool because of its high spatial resolution and its insusceptibility to cloud and solar light conditions. Recent studies[15, 16] showed that satellite-based synthetic aperture radars (SAR) could also provide valuable information about fronts in the ocean. This information can not only supplement data from optical sensors but also, in many cases replace it. A use of satellite radar data in the research of small- and mesoscale fronts in inland seas allowed to significantly improve our understanding of their generation, propagation and decay. According to the paper[4] one of the most critical aspects of physical oceanography is a front mapping and characterization.

During our long-term monitoring of the Baltic Sea, we came across a significant number of surface manifestations of various fronts in satellite imagery. In this paper we: (1) demonstrate the capability of SAR as a tool for fine scale marine surface analyses and for detecting of sub-mesoscale fronts of various types; (2) present examples of fronts commonly detected in the SAR data of the study region; (3) correlate the fronts with atmospheric and oceanic forces on the base of SAR data; (4) explore the SAR signatures of fronts of various origin.

THE STUDY REGION

Our study region is the south-eastern part of the Baltic Sea (see Fig.1). The Baltic Sea is a marginal sea of the Atlantic Ocean. Water exchange of the Baltic Sea carried out by a complex system of big as well as small and narrow straits connecting it with the North Sea is slow: it takes about 30-50 years for the complete renewal of water. Baltic Sea is a shallow shelf sea. Its mean depth is only 48 m, and the maximal depth is 459 м (in the point with coordinate 58°35' N, 18°14' E). The depths up to 50 m predominate, accounting for 60% of the sea surface area. The Baltic Sea is a non-tidal sea that is having no tidal flows. The tide-induced sea level variations are minimal: from 4 cm (Klaipeda) to 10 cm (Gulf of Finland), and within the Baltic proper ordinary tides are scarcely perceptible. The sea has a peculiar configuration what affects the formation of features of the wind-wave regime of the south-east coast.

In the southeastern part of the Baltic Sea, the Gulf of Gdansk is located into which Vistula (one of the principal rivers of the Baltic basin) flows, as well as two practically closed brackish water lagoons: the Vistula Lagoon also known as the Vistula Bay or the Vistula Gulf, and the Curonian Lagoon.

a b

Figure 1. a) A map of the Baltic Sea. Red rectangle outlines the location of the area of interest; b) A map of the area of interest.

DATA AND DATA PROCESSING

The front dynamics survey was based on combined use of satellite imagery obtained by sensors installed on various satellites and operating in different bands of electromagnetic waves. Data in visible, infrared and microwave ranges provided the primary material for the analysis.

We used high-resolution radar imagery data obtained by SARs onboard Envisat, Sentinel-1A, B, TerraSAR-X, and RADARSAR-2 satellites. Processes occurring on the fronts and in the frontal zones have the most diverse characteristics and scales, and it is not always possible to pinpoint typical features that would allow us to detect them in satellite images with 100% confidence. For more robust interpretation, the SAR data is complemented by other satellite data on the sea surface and water condition, sea surface temperature, and mesoscale water dynamics. We used data in visible and IR bands taken by Envisat MERIS, Terra/Aqua MODIS and by scanning radiometers of Landsat-5, 7, 8 satellites.

The data were processed and analyzed using the toolkit of the satellite information system developed at the Space Research Institute of the Russian Academy of Sciences (IKI RAS). The system is named "See the Sea" (STS). STS functionality is detailed in[17]. STS provides not only instruments for fast and easy access to satellite data and products, but also various tools for specialized data analysis. STS enables easy search of the distributed image archive using a sensor type, a time interval, and a location as search criteria. The selected image is visualized in the map area of the interface along with its geographic basis and related cartographic data. All information (regardless of sensor type or product) is presented for viewing in the same cartographic projection for a given geographic area. This facilitates the selection of data for analysis. Combining data of different nature (active/passive microwave, VIS, and NIR), spatial resolution and swath width allows better understanding the complex nature of meteorological and hydrodynamic processes in the study regions, and revealing the factors favoring generation, evolution, and decay of fronts. The main characteristics of fronts were determined using the STS interface, in an interactive semi-automatic mode. As a result, we have a comprehensive description of the phenomena stored in the database. The database tools allow storing and visualization of graphical and attributive information, hierarchical classification of observed processes, searching by spatial, time and typological criteria, and mapping fronts in the area of interest.

RECOGNIZING FRONTAL TYPES IN SAR IMAGERY

SAR images carry information about various phenomena that occur both in the near-surface layer and in the depths of the ocean. Microwaves penetrate a water column by as much as a few millimeters as the most; therefore, processes, taking place in the ocean deeper than that are possible to visualize solely from their surface manifestations. Ripples caused by the near-surface wind reflect both atmospheric and bulk oceanic processes that in some way or other modulate short gravity-capillary waves at the ocean surface. This effect is, in turn, manifested as modulation of the backscattered radar signal. In such a manner SAR images of the ocean surface visualize both oceanic and atmospheric motions. Microwaves have a significant advantage over electromagnetic waves of other ranges because they can penetrate through cloud cover and thus render round-the-clock observations of the ocean regardless of weather conditions. Another strength of microwaves, important for remote sensing of the ocean, lies in the fact that they resonantly interact with surface perturbations and thereby visualize such motions in the ocean that are impossible to observe using electromagnetic waves of other frequency ranges. The uniformity of the dielectric properties of the sea surface greatly facilitates the analysis of the SAR images and makes it possible to link the intensity of the backscattered signal with the characteristics of the ocean surface roughness[18].

Fronts of different origin are frequently visible in SAR images of the sea surface. These can be sea surface signatures of oceanic fronts as well as of atmospheric fronts. The fronts and frontal zones are characterized by sharp spatial changes in the thermodynamic characteristics of the marine environment and, consequently, spatial gradients greater than those in the surrounding waters. Speed shifts contribute to the appearance of areas of weakness or amplification of short surface waves. Therefore, the wave field on both sides of the front can have different wave characteristics that SAR is capable of registering.

2.1 Manifestation of atmospheric fronts in SAR images of the sea surface

Fronts are a characteristic feature of the circulation in the atmosphere as well as in the ocean. However, the significant differences between these two environments (by their physical parameters, equations of state, types of stratification, scaling factors, etc.) do not allow us to expect a one hundred percent analogy between atmospheric and oceanic fronts.

It is surprising that despite the abovementioned differences, the oceanic and atmospheric fronts have many similarities both in their dynamics and in the very process of their formation.

The first and foremost problem in study of fronts using SAR imagery is to discriminate between the signatures of fronts in the sea and those in the near-surface layer of the atmosphere. Atmospheric fronts are manifested in SAR images of sea surface because the front induced variations of near-surface wind velocity and wind direction modulate surface roughness and hence modulate the radar backscattering. Some examples of imprints of atmospheric fronts in SAR images are presented in[19, 20]. The paper[21] provides a comprehensive review of the signatures of synoptic atmospheric fronts imaged by SAR, including warm fronts, cold fronts, occluded fronts, and secluded fronts. We, nevertheless, are interested in atmospheric fronts of scales smaller than those presented in[21].

Hereafter we examine SAR signatures of atmospheric fronts that differ in types. Three case studies are provided, based on SAR imagery, registered during our survey of the southwest Baltic Sea. Below it is shown in what a way SAR can reveal mesoscale and small-scale patterns of cold fronts, warm fronts, and occluded fronts. Particular attention is paid to the capability of SAR to reveal small-scale and mesoscale features of atmospheric fronts. The SAR signatures specific for different frontal types will be outlined that can be used for the identification of fronts by their kind. These features are not usually detectable using traditional observational data of optical sensors because of their small dimensions and because upper-level clouds often mask them.

2.1.1 Case 1: Cold atmospheric front

A cold front in the atmosphere is often defined as the changeover region between the advancing cold air mass and receding warm air mass[22]. Cold fronts occur when warm air is pushed up into the atmosphere by colder air at the ground. Sometimes a cold front is seen as a significant intrusion of cold air into warm air in the form of gravity current having an extremely unstable boundary[23].

On July 11, 2016, the South-Eastern Baltic was on the periphery of the region of low atmospheric pressure with the center over the North Sea. Weather conditions were formed under the influence of atmospheric fronts. The surface analysis maps[24] for 06:00 UTC and 12:00 UTC on 11 July 2016 depicted in Figs. 2, 3 display a cold atmospheric front moving through the study area in the northeastern direction.

The passage of the cold front was registered on that day in two different SAR images. Signatures of the cold front leading edge are seen in the Sentinel-1A SAR image taken at 04:59 UTC in the western part of the study area and in the RADARSAT-2 SAR image taken at 16:35 UTC eastward of the Gotland Island (see Figs. 2a, 3a). The front line in both SAR images is made evident by a sharp jump in the amplitude of the backscattered signal. The inset graphs depicted in Figs. 2b, 3b show variations in radar signal across leading edge of the front. Higher backscatter is found at the rear of the front. Cross-frontal jumps in the amplitude of the backscattered signal are 5 dB and 3 dB correspondingly. The pink areas in the graphs mark the locations of radar backscatter jumps at the leading front edge.

Bright bands of enhanced radar backscattered ahead of the front seen in the Sentinel-1A SAR image acquired on 11 July at 04:59 UTC (Fig. 2a) are imprints of the squall line, where winds are gusting to gale force as the front approached. Footprints of intensive thunderstorm rains are also visible ahead of the moving front in this image. The thunderstorms and heavy rains occur immediately before a cold front due to cumulonimbus clouds formation in the result of rapid air convection often preceding the cold front in summer. Thick rainy clouds appear in the SAR image as bright structures of the increased backscattered signal. Rain becomes visible on SAR image of the ocean because impinging rain drops modify the short-scale sea surface roughness and generate splash products and because raindrops in the atmosphere scatter and attenuate the radar beam[25]. A zone of enhanced backscatter visualizing squall lines ahead of front is one of the characteristic features of cold front manifestations in SAR images of the sea surface.

The leading edge of a cold front looks uneven in the SAR image of the sea surface, and consists of a series of lobe and cleft instabilities. Clefts may be described as V-shaped indentations in the front that propagate and merge along the front, and lobes may be described as a series of localized bursts along the front that appear as projecting noses with bulges or buttresses which continually change shape[26]. Figures 2d and 3d provide examples of these phenomena showing detailed structure of the leading front edge. The existence of lobe and cleft patterns indicates that the corresponding SAR frontal signature is that of a cold front.

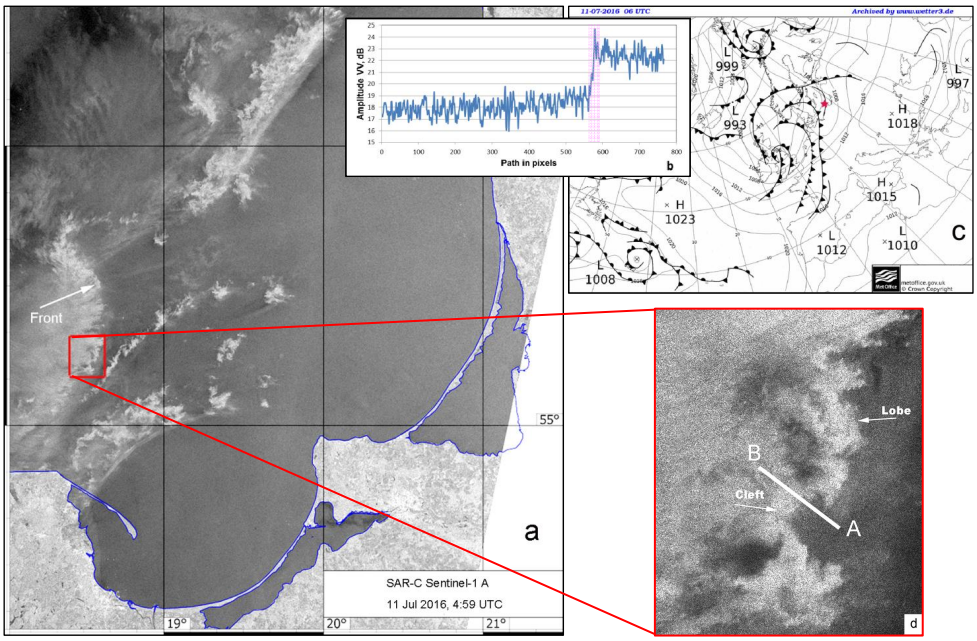

Figure 2. a) A part of the Sentinel-1A SAR image of a cold front in the marine atmosphere over the southeastern Baltic Sea taken on 11 July 2016 at 04:59 UTC. The front is oriented north–south and moving toward the northeast; b) Variations in radar signal along the transect across the front leading edge; c) UK MetOffice surface analysis valid at 06:00 UTC 11 July 2016. Red star shows the SAR image placing. d) Zoomed SAR image showing detail of the leading front edge. The variations in the radar backscatter shown in (b) were taken along the white line AB.

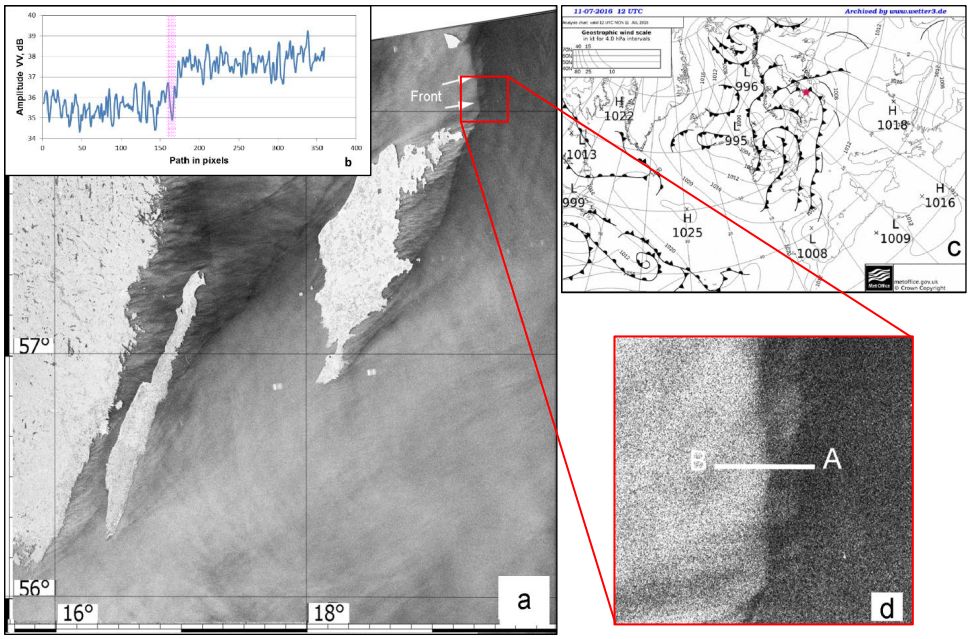

Figure 3. a) A part of the RADARSAT-2 SAR image of a cold front in the marine atmosphere over the Baltic Sea eastward of the Gotland Island taken on 11 July 2016 at 16:35 UTC. The front is oriented north–south and moving toward the northeast; b) Variations in radar signal along the transect across the front leading edge; c) UK MetOffice surface analysis valid at 12:00 UTC 11 July 2016. Red star shows the SAR image placing. d) Zoomed SAR image showing detail of the leading front edge. The variations in the radar backscatter shown in (b) were taken along the white line AB.

2.1.2 Case 2: Warm atmospheric front

A warm atmospheric front occurs when warm air pushes cooler air away from the surface. The warm front moves towards colder air and is followed by a warm air mass.

On November 5, 2016, weather conditions the South-Eastern Baltic were formed under the influence of a cyclone with the centre over the North Sea. The passage of a warm atmospheric front over the test area was registered. The near-surface wind field was inhomogeneous in speed and direction. In the northern part of the area of interest, ahead of the front line, the wind speed reached 15 m/s. The heavy cloudiness was observed.

Signature of the leading edge of this warm atmospheric front was captured in the RADARSAT-2 SAR image taken over the south-eastern Baltic Sea at 04:56 UTC on 5 November 2016. Figure 4a is the SAR image. The front line in this image is made evident by a sharp drop of the backscattered signal. The inset graph depicted in Fig. 4b shows variations in backscattered signal across the leading edge of the front. Lower backscatter is found at the rear of the front. Cross-frontal drop in the amplitude of the backscattered signal is about 3 dB. The pink area in the graph marks the location of radar backscatter drop at the leading front edge.

The surface analysis map[24] for 06:00 UTC on 05 November 2016 presented in Fig. 4c displays a warm atmospheric front moving northward through the study area.

The SAR signature of the warm front boundary looks smoother than those of the cold front discussed above. It meanders in response to small-scale vortices. This frontal "waviness" is assumed to be a result of horizontal shear instability[27]. Another characteristic feature of the SAR signature of a warm front is the existence of quasi-linear bands of smooth amplification and attenuation of backscattered signal aligned nearly perpendicular to the front and extending about 10 − 15 kilometers to the front cold side (see Fig. 4d). These structures are SAR signatures of shear-driven gravity waves.

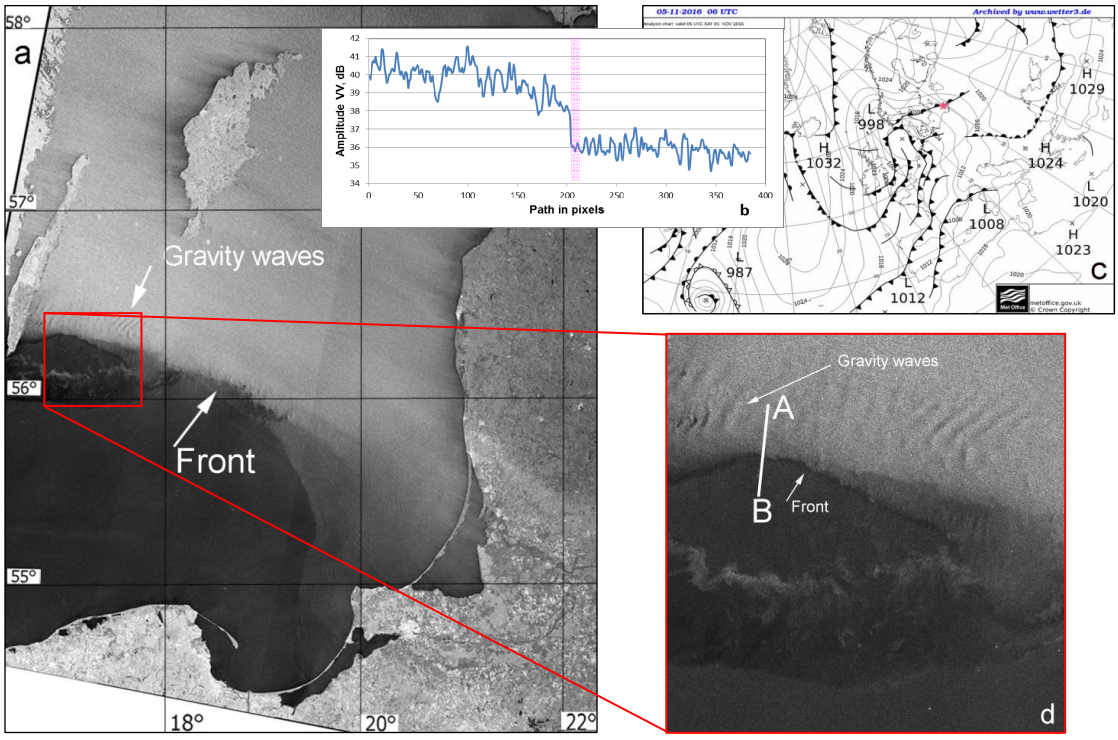

Figure 4. a) A part of the RADARSAT-2 SAR image of a cold front in the Baltic Sea taken on 5 November 2016 at 04:56 UTC. The front is oriented west–east and moving northward; b) Variations in radar signal along the transect across the front leading edge; c) UK MetOffice surface analysis valid at 06:00 UTC 5 November 2016. Red star shows the SAR image placing. d) Zoomed SAR image showing detail of the leading front edge. The variations in the radar backscatter shown in (b) were taken along the white line AB.

2.1.3 Case 3: Occluded front

Occluded fronts appear when a mass of cold air reaches a mass of warm air and pushes it up, which makes the warm air hidden, or "occluded." This situation takes place often when a cold front moves faster than a warm front and overtakes it. Sometimes occluded fronts could be hardly distinguished from warm fronts based on SAR imagery alone as they have many common features in their SAR manifestations. Like warm fronts, occluded fronts are generally smooth except where they meander in response to mesoscale vortices. Moreover, SAR signatures of atmospheric gravity waves are also sometimes observed with occluded fronts.

On December 11, 2016, a low atmospheric pressure zone was located over the South-Eastern Baltic. The sky was overcast. The surface analysis map[24] for 06:00 UTC on 11 December 2016 presented in Fig. 5 displays an occluded atmospheric front. The front is oriented northwest-southeast and is moving toward the northeast.

Figure 5a shows a TerraSAR-X image taken over the south-eastern Baltic Sea at 04:50 UTC on 11 December 2016. Signature of the leading edge of an occluded atmospheric front is distinctly seen in the image. The graph depicted in Fig. 5b shows variations in backscattered signal across the leading edge of the front. The backscattered signals ahead of and behind the front are comparable in their magnitudes. On the front line, however, signal experiences a drop-off and the front line in the SAR images is seen as a thin curved strip of low backscatter. The pink area in the graph marks the area of the sharp decrease about 20 dB in the amplitude of the backscattered signal at the leading front edge.

Signatures of gravity waves in the marine atmosphere are also seen in the SAR image ahead of the occluded front; however, they are oriented at a more acute angle than in the case of a warm front discussed above.

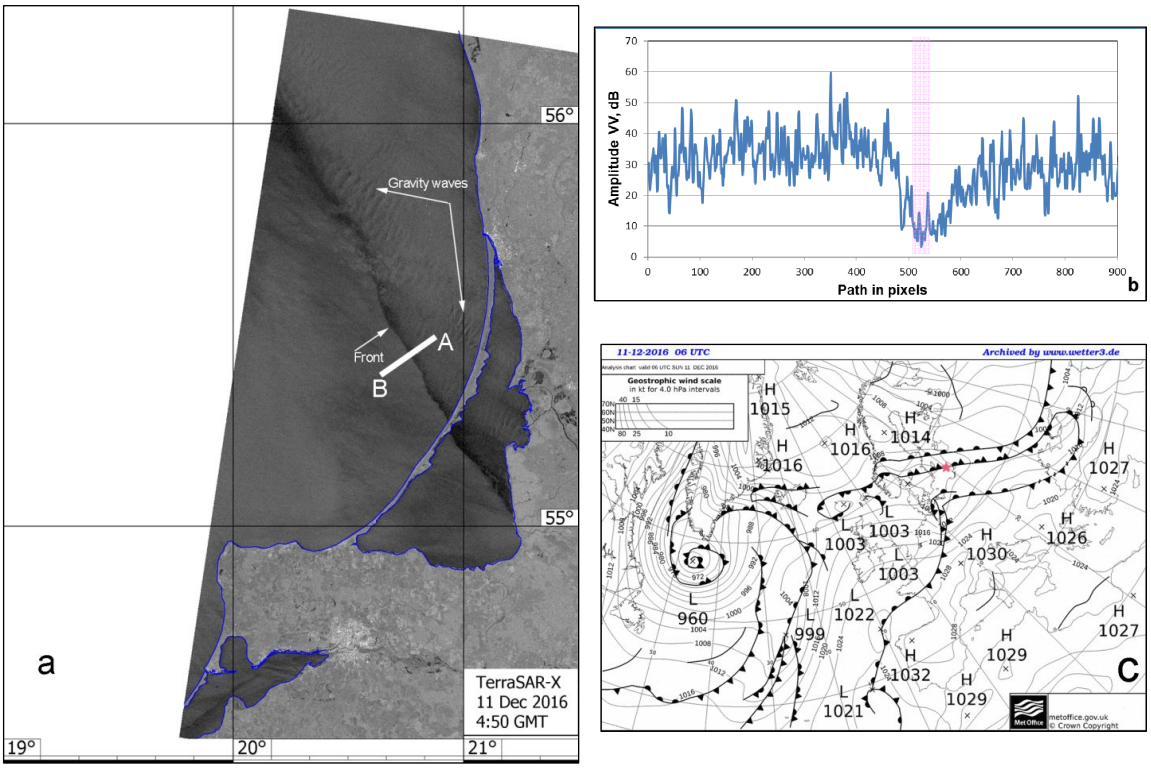

Figure 5. a) A part of the TerraSAR-X image of a of a well-defined occluded front with gravity waves in the marine atmosphere over the southeastern Baltic Sea taken on 11 December 2016 at 04:50 UTC. The front is oriented northwest–southeast and moving toward the northeast; b) Variations in radar signal along the transect across the front leading edge; c) UK MetOffice surface analysis valid at 06:00 UTC 5 November 2016. Red star shows the SAR image placing. d) Zoomed SAR image showing detail of the leading front edge. The variations in the radar backscatter shown in (b) were taken along the white line AB.

2.2 SAR manifestations of small scale fronts in the shallow sea

Frontal features visible in radar images of the sea surface quite often are sea surface manifestations of oceanic fronts. Oceanic fronts, as well as fronts in the atmosphere over the ocean, are visible in SAR images due to a change of the small-scale sea surface roughness responsible for the radar backscattering. There are several hydro-physical mechanisms connected with oceanic fronts that result in a modulation of the sea surface roughness: (i) wave-current interaction; (ii) damping of the gravity-capillary component of surface waves by surface films; (iii) changes in the stability of the air-sea boundary layer.

By their very nature, oceanic fronts are associated with a convergent flow, which brings fluid of different properties into the frontal region. Fronts can be visible at the sea surface as delimitation lines visualized by (i) rough water or slicks (smooth surface); (ii) accumulation of debris or foam; (iii) abrupt change of sea surface temperature or color. Rough water is frequently observed when there is a significant current shear across the front. Slicks may be caused by the damping effect of surface films accumulated in the convergence zones. Accumulation of debris and foam arises from the convergence of surface currents at a front.

Below, we examine SAR manifestations of sea fronts, which are made visible in SAR data due to various mechanisms of front effects on the disturbed sea surface. We focus on the small-scale fronts, which are often short-lived and have narrow frontal interfaces.

2.2.1 Case 1: River plume fronts

Plume fronts can be found in areas where fresh water from the river mouth discharges into the ocean or a sea. These fronts mark the boundary between the surface layer of buoyant fresh water and the denser salty marine water near the river mouth. Plume fronts are narrow zones of significant horizontal density gradients at the sea surface. They may be associated with a substantial variation in color, turbidity, or to regions of foam and detritus accumulation.

Numerous satellite observations of river plumes were reported, and results of their studies published[28, 29, 30, 31]. In these studies, spatial patterns associated with the river plume are mainly linked to the phase of the tide in the outflow area, and general characteristics of the structure and evolution of a river plume subjected to the action of strong tidal currents.

We explore river plumes formed in the non-tidal sea. Fronts of this kind are often observed in the satellite data of the Gulf of Gdansk and are formed by the Vistula outflow.

Since the end of the 19th century, the Vistula flows into the Gdansk Gulf through a straight, human-made channel. Such direct inflow of the river results in the fact that river and sea waters mix right in the bay without any intermediate estuary or another transitional water body. Previous oceanographic studies showed that the Vistula plume might extend up to 9–27 km from the river mouth and that its vertical extension might range from 0.5 m to 12 m, depending mainly on the wind speed and direction, as well as a combination of factors such as the river water discharge rate, sea level and the duration of their interactions[32].

Particularly striking examples of Vistula River surface front signatures in satellite images were obtained during intense and devastating flooding in Poland along the Vistula River in May-July 2010. Floodwaters reached the river mouth on the night of 25/26 May and aftereffects of this vast discharge were observed for several weeks.

Two SAR images of the Gdansk Bay are depicted in Fig. 6. The SAR image of Fig. 6a was taken at 20:25 UTC on 28 May 2010 when the inflow of large amounts of highly turbid floodwater to the sea just started. The SAR image of Fig. 6c was taken about nineteen days after that, at 09:01 on 16 June 2010, when the inflow of turbid river water weakened. In both images, the Vistula surface front is clearly seen.

Sea surface patterns associated with the Vistula River plume can be distinctly seen in the center of the SAR image presented in Fig 6a. It is the large almost circular area where the radar backscatter is slightly higher than in the outer region. The plum area is enclosed by a narrow bright line, which is a SAR signature of a frontal line. The frontal line is characterized by mostly enhanced radar backscatter. The frontal line is better pronounced in the eastern semi-circumference, while in the western part the frontal line is partly imaged as a zone of enhanced/reduced backscatter. The enclosed plum has the area about of 630 km^2. In Fig. 6d the well pronounced almost semi-circular frontal line encloses a region with the area of about 125 km^2. The plume area is characterized in this case by nearly the same intensity of radar backscatter as the outer surroundings.

The inset graphs (Figs 6b, 6e) show variations in radar signal along the cross-sections of the fronts (white lines). The pink areas mark the regions of enhanced radar backscatter corresponding to the Vistula surface front. In the profiles, the sea surface manifestations of the Vistula surface fronts are visible as regions of enhanced radar backscattering. The width of the frontal line was about 400 m on 25 May 2010 and about 750 m on 6 June 2010. The jump in the radar backscatter amplitude on the front was better pronounced on 25 May 2010. The relative variations of radar signal on the front are approximately 1.5 dB and 3 dB correspondently. In this case, the changes in surface roughness on the surface front boundaries are due to interactions of short surface waves with surface current gradients. These interactions are manifested as thin bands of enhanced backscattering in the images and are caused by an increase of the surface roughness at the front. We think that the observed difference in the radar signal modulation on the plume front is caused mostly by the orientation of the front with respect to the wind direction. The same result was reported in the paper[33] for SAR signatures of internal solitary waves.

For more robust interpretation, SAR data were analyzed jointly with data of optical sensors. River plumes are best manifested in images acquired by satellite optical sensors. Examples of river plume manifestations are shown in Figs.6 b,d. These figures depict charts of Total Suspended Matter (TSM) calculated on the base of MERIS Envisat data taken simultaneously with the SAR images shown in Figs 6a, 6c. Plume areas different in their turbidity can be readily distinguished[34]. On May 28, 2010, the plume had large dimensions and reached the Hel Spit. On June 6, 2010, waters were located near the Vistula mouth, the plume area decreased by almost fivefold.

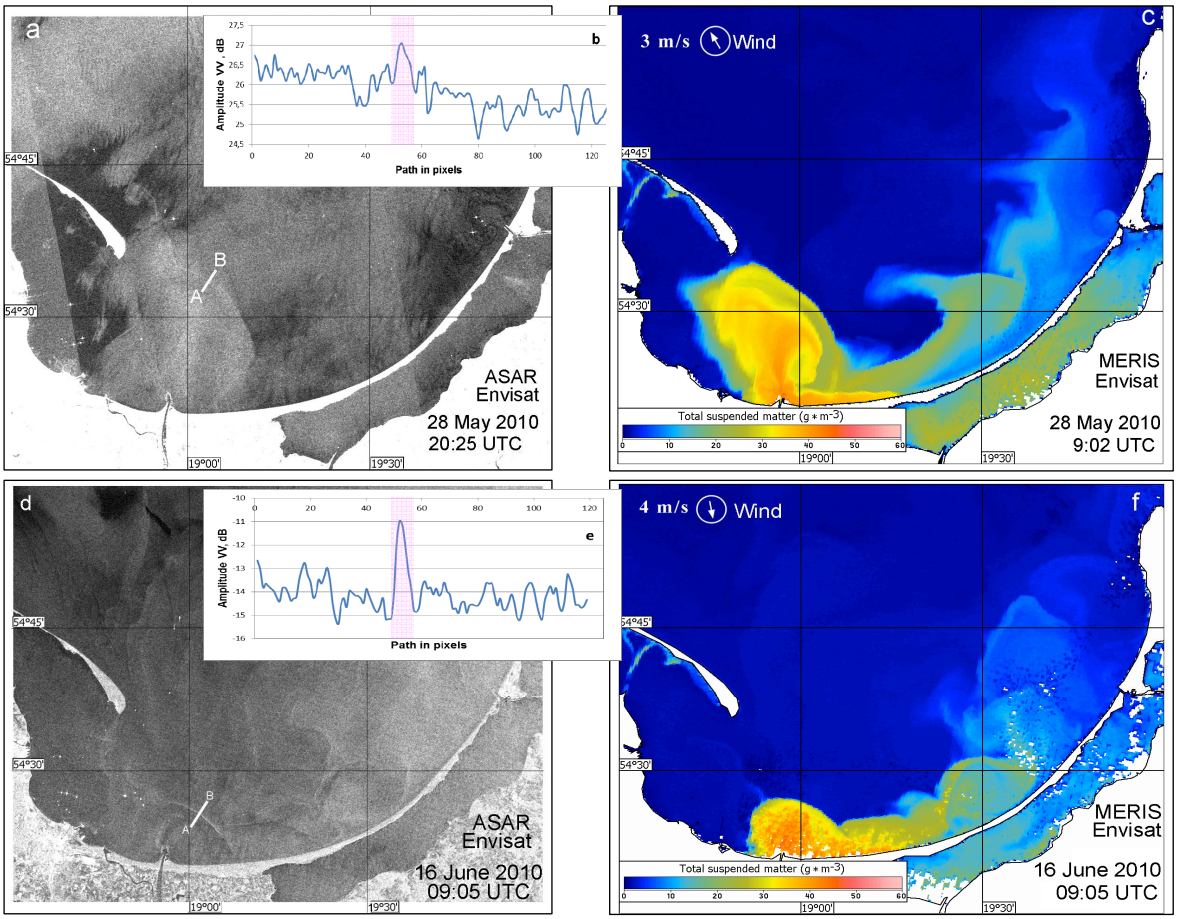

Figure 6. a) A part of the Envisat ASAR image taken over the Gulf of Gdansk on 28 May 2010 at 20:25 UTC. Along the white line inserted into this image the variations in the radar backscatter are determined; b) Variations in radar signal along the transect across the Vistula surface front leading edge; c) Suspended matter chart derived from Envisat MERIS data taken over the Gulf of Gdansk on 28 May 2010 at 09:02 UTC; d) A part of the Envisat ASAR image taken over the Gulf of Gdansk on 16 June 2010 at 09:05 UTC. Along the white line inserted into this image the variations in the radar backscatter are determined; e) Variations in radar signal along the transect across the Vistula surface front leading edge; f) Suspended matter chart derived from Envisat MERIS data taken over the Gulf of Gdansk on 16 June 2010 at 09:05 UTC.

2.2.2 Case 2. Frontal slicks in a coastal zone

Slicks represent a frequently detected pattern in SAR imagery. Primary mechanism of slick formation is a surfactant accumulation in small-scale convergence zones. Fronts in SAR images are seen as solitary elongated slicks. Modulation of centimeter- and decimeter-scale surface waves caused by redistribution of surface films by currents associated with sea fronts can be the dominant factor behind the surface manifestation of fronts in the sea imaged by SAR operating in short centimeter wavelengths. Elongated areas with increased film concentrations are present on the sea surface in the convergent zone at the front boundary resulting in significant attenuation of ripples and formation of slicks.

Figure 7a depicts a part of the RADARSAT-2 SAR image taken over the Gulf of Gdansk on 04 August 2016 at 16:35 UTC. A single elongated slick of northwest-southeast orientation with the length of about 50 km and width 0.5 to 1 km is distinctly visible in the SAR image. This slick exhibits a surface manifestation of a hydrological front developing in shallow water.

The graph presented in Fig. 7b depicts variations in backscattered signal across the leading edge of the front. The backscattered signals ahead of and behind the front are comparable in their magnitudes. On the slick, which manifests the frontal line, the signal experiences a drop-off. The pink area in the graph marks the sharp decrease about 4 dB in the amplitude of the backscattered signal at the leading front edge.

This hydrological front separates the highly turbid coastal water and the cleaner water of the Gdansk Gulf. The high water turbidity results from Vistula inflow. Prolonged winds from north-east direction decrease the extension of river water in the Gulf. The flow of Vistula water being oppressed, no river plume is formed in the Gulf of Gdansk, and river water is distributed along the shores. The turbid waters are trapped in the area between the coastal and frontal line, remaining there for some time. Such a situation favors the accumulation of substances carried by Vistula water in the coastal area.

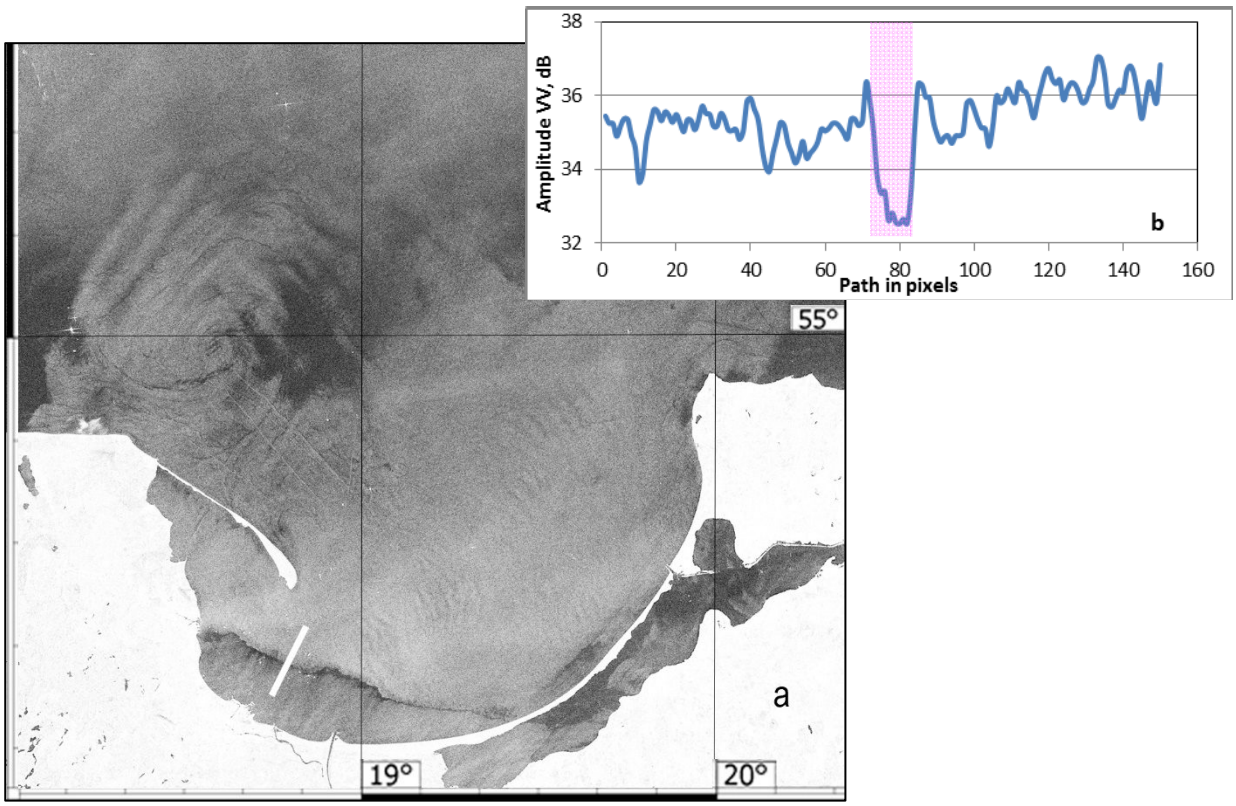

Figure 7. a) A part of the Radarsat-2 SAR image taken over the Gulf of Gdansk on 04 August 2016 at 16:35 UTC. The variations in the radar backscatter are determined along the white line; b) Variations in radar signal along the transect across the front leading edge.

2.2.3 Case 3: Small-scale thermal fronts

Cloudiness of the Baltic Sea region is a significant limitation for observing the sea surface from space in the optical range. In this connection, SAR data which is independent of cloudiness and sun illumination provides an additional source of information on the sea surface conditions, including the information on the presence of thermal fronts of various scales. The capability of SAR to reveal inhomogeneity of the sea surface temperature (SST) has been confirmed in previous studies[35, 36].

Frontal zones with strong surface temperature gradients can separate oceanic regions with the different stability of the atmospheric boundary layer (ABL) above them. The transformation of the atmospheric boundary layer over the frontal zone with strong temperature gradients can affect the radar backscatter pattern. "In the case of radar cross-section, changes over SST fronts of small horizontal width, the change in atmospheric stability is the primary bulk quantity undergoing an immediate response to the change in sea surface temperature"[35]. This situation can often be observed when the wind speed is low, and the temperature difference between the sea surface and the near-surface air is small. In these cases, the stable stratification of the air-sea boundary layer develops over colder water and the unstable or neutral – over warmer water.

The transformation of the ABL over the thermal front can be seen in the RADARSAT-2 SAR image taken on 12 November 2016 at 04:52 UTC (see Fig. 8a). The weak north-eastern wind was blowing in the test area at the time of the SAR image acquisition. The air temperature field was homogenous in the test area (see Fig.8b). None of the atmospheric fronts were registered moving through the test area.

Distinct spatial changes in SAR image clatter patterns, which strongly depend on the type of stratification of the atmospheric boundary layer, are observed due to the presence of meandering SST front (Fig.8c). An unstable stratification of the boundary layer occurs in areas where the sea surface is warmer than the near-surface air. Under unstable stratification, we observe surface manifestations of convective motions in the near-surface layer[36, 37, 38, 39]. These structures correspond to atmospheric convection cells 2.5 to 25 kilometers in size. Cell sizes and the intensity of convective processes in the near-surface atmosphere depend on the degree of the thermodynamic instability.

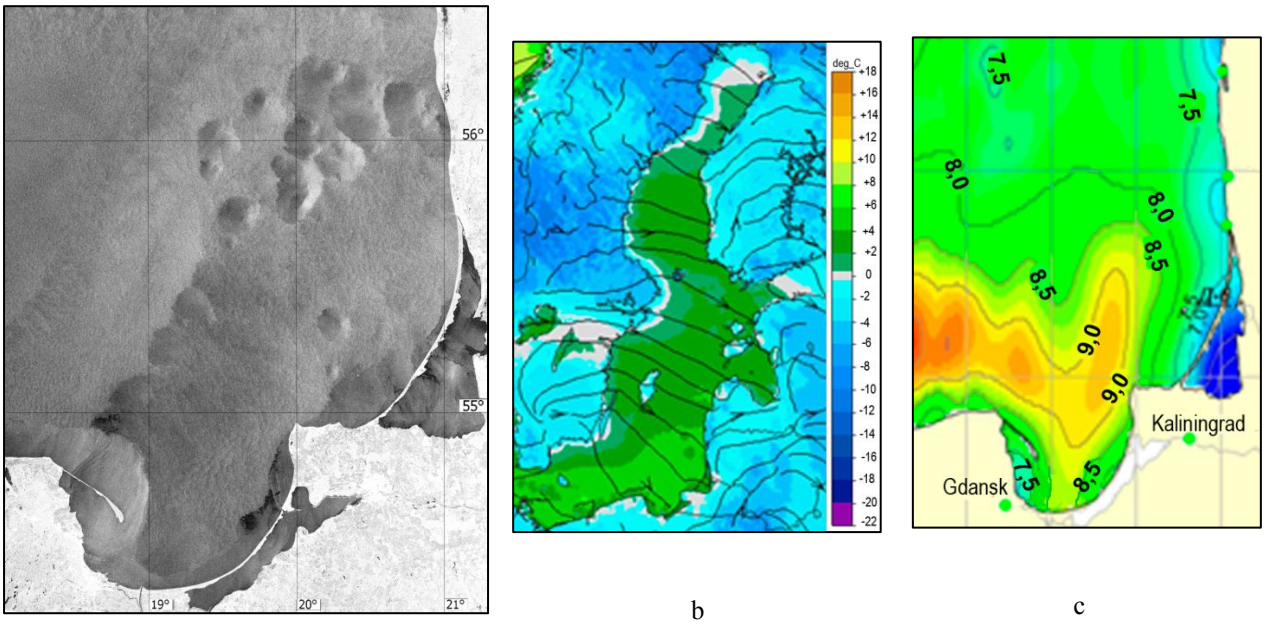

a b c

Figure 8. a) A part of the RADARSAT-2 image taken over the South-Eastern Baltic Sea on 12 November 2016 at 04:52 UTC; b) An air temperature chart in the Baltic Sea region for the 12 November 2016; c) A part of an SST chart for the 12 November 2016.

The example above has demonstrated the capability of the sea surface radar imagery to reveal changes in the type of ABL stratification caused by an SST front in the presence of a near-uniform field of the near-surface air temperature. Hereafter we examine a case of ABL modulation due to a change in the temperature of the near-surface air in the presence of a uniform SST field.

The transformation of the ABL is seen in the Sentinel-1A SAR image taken on 27 November 2016 at 04:51 UTC (see Fig. 9a). At the time of the SAR image acquisition, weather conditions in the South-Eastern Baltic were formed under the influence of a cyclone with the center over the Saint-Petersburg region. The wind was blowing from the north-west at 12-13 m/s (Fig. 9b). In the test area, the SST field was almost homogenous with the average temperature of approximately 7.5°C (Fig. 9c). A nearly horizontal line is distinctly seen in the SAR image separating it into two regions. Surface manifestations of intensive convective motions in the near-surface atmosphere are seen in the top half of the SAR image. The cellular elements in the SAR images are the surface manifestations of convective cells in the near-surface atmosphere and can be considered an indicator of the unstable stratification of the air-sea boundary layer. This can occur if the temperature of the sea surface is higher than that of the near-surface air. Sizes of convective cells increase from 4 km near the borderline up to 20 km in the top of the image. The bottom half of the image bears no imprints of the convective motions in the near-surface atmosphere. The location and the shape of the boundary line approximately correspond to that of the 6°C isotherm on the chart of the near-surface air temperature. The sea surface is warmer than the near-surface air when the air temperature is lower than 6° C, and the boundary layer becomes unstable, and conditions are created for the atmospheric convection development.

While two cases discussed above highlight the success of SAR imagery in capturing the boundary layer stability change, they also illustrate some limitations of this technique. Based on the SAR data only, we are not able to pinpoint the cause of the ABL modulation. I.e. we're not able to reveal if it is caused by a change in the SST in the presence of a nearly uniform atmospheric temperature field or by a change in the temperature of the near-surface air in the presence of a uniform SST field.

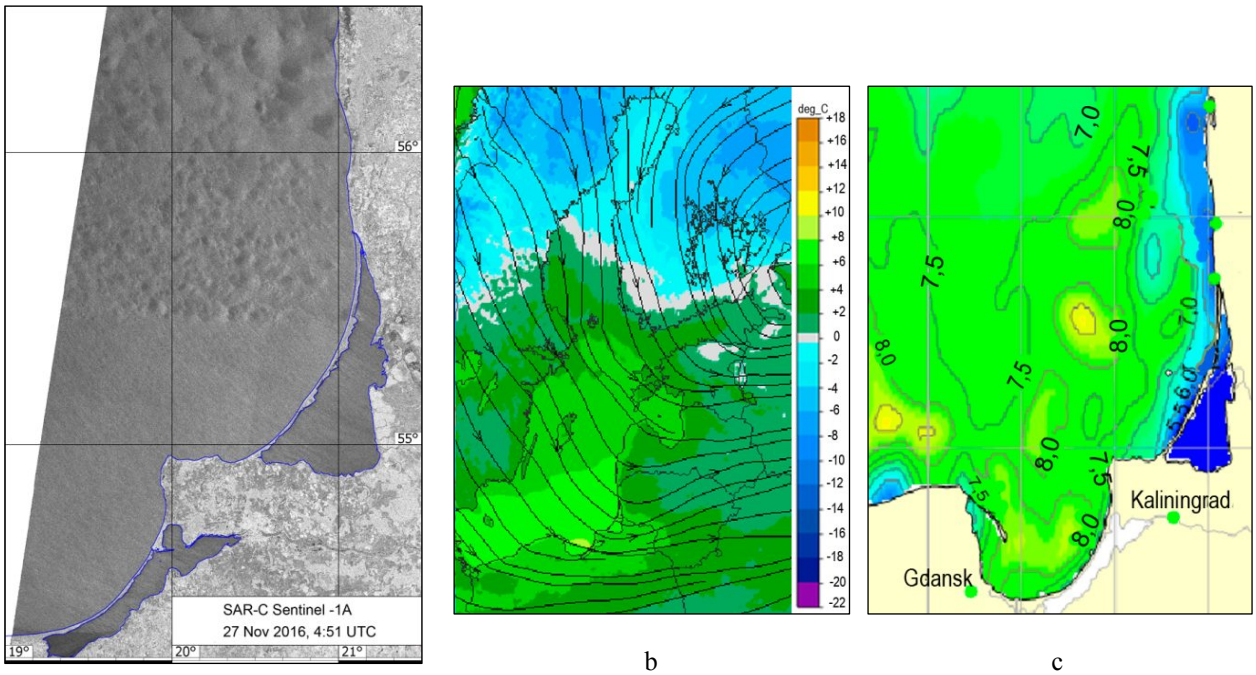

Figure 9. a) A part of the Sentinel-1A SAR image taken over the South-Eastern Baltic Sea on 27 November 2016 at 04:51 UTC; b) An air temperature chart in the Baltic Sea region for the 12 November 2016; c) A part of a SST chart for the 12 November 2016.

CONCLUSIONS

In this paper, we examine surface manifestations of submesoscale fronts of various origins visible in SAR images of the South-Eastern Baltic. We demonstrate the usefulness of SAR imagery for the study of fronts in both the sea and the atmosphere over the sea. Fronts of both types are visible in SAR images due to a change of the small-scale sea surface roughness responsible for the radar backscattering. Our first goal is to discriminate between signatures of fronts in the sea and those in the near-surface layer of the atmosphere. We accomplish this by utilizing the supporting data, such as meteorological maps, sea surface wind maps, SST and TSM charts derived from data of space-borne sensors operating in visible and IR bands.

We outline the SAR signatures that differ between frontal types and contribute to the identification of fronts by their nature. We point out that many mesoscale features that are associated with fronts of different nature are not usually detectable using traditional observational data sources because of their small scale and because upper-level clouds often mask them.

The use of satellite remote sensing methods and SAR data in particular, makes it possible to obtain information on the frequency and spatial distribution of submesoscale fronts in test areas, identify possible mechanisms of their generation and factors that determine their evolution and decay, and reveal typical velocities of their movement, seasonal and inter-annual variability.

ACKNOWLEDGEMENTS

The research on submesoscale fronts in inner seas was supported by the Russian Science Foundation under the project # 14-17-00555. The development of the See the Sea information system for the satellite data processing and analysis is supported by the "Monitoring" theme, registration no. 01.20.0.2.00164. This system is functioning with use of the data from the "IKI Monitoring" center for collective use.

REFERENCES

[1] Fedorov, K. N., [The physical nature and structure of oceanic fronts], Springer, 1-333 (1986).

[2] Ginzburg, A. I., Kostianoy, A. G., [Oceanography-Volume 1], EOLSS Publishers Co, Oxford, 237-267 (2009).

[3] Kostianoy, A. G., Nihoul, J. C. J., Rodionov, V. B., [Physical Oceanography of Frontal Zones in the Subarctic Seas Volume 71], Elsevier, 1-316 (2004).

[4] Belkin, I. M., Cornillon, P., C., Sherman, K., "Fronts in Large Marine Ecosystems," Progress in Oceanography 8(1–4), 223-236 (2009).

[5] Bisagni, J. J., Kim, H.-S., Chaudhuri, A., "Interannual Variability of the Shelf-Slope Front Position Between 75 and 50 W," Journal of Marine Systems 78(3), 337-350 (2009).

[6] Legeckis, R., Brown, C. W., Chang, P. S., "Geostationary satellites reveal motions of ocean surface fronts," Journal of Marine Systems 37(1–3), 3–15. (2002).

[7] Belkin, I. M., Cornillon, P. C., Ullman, D., "Ocean fronts around Alaska from satellite SST data," Proc. American Meteorological Society 7th Conference on the Polar Meteorology and Oceanography, 12–15 (2003).

[8] Belkin, I. M.,Cornillon, P. C., "Bering Sea thermal fronts from Pathfinder data: seasonal and interannual variability," Pac. Ocean 3(1), 6–20 (2005).

[9] Belkin, I. M.,Cornillon,P. C., "SST front of the Pacific coastal and marginal seas," Pac. Ocean 1(2), 90–113 (2003).

[10] Miller, P., "Multispectral front maps for automatic detection of ocean colour features from SeaWiFS," Int. J. Remote Sensing 25, 1437–1442 (2004).

[11] Miller, P., "Composite front maps for improved visibility of dynamic sea-surface features on cloudy SeaWiFS and AVHRR data," J. Mar. Systems 78, 327–336 (2009).

[12] Ullman D., Cornillon P. C., "Continental shelf surface thermal fronts in winter off the northeast US coast," Continental Shelf Research 21(11–12), 1139-1156 (2001).

[13] Kahru, M., Hakansson, B., Rud, O., "Distribution of the sea-surface temperature fronts in the Baltic Sea as derived from satellite imagery," Cont. Shelf Research 15, 663–679 (1995).

[14] Wang, D., Liu, Y., Qi, Y., Shi, P., "Seasonal variability of thermal fronts in the northern South China Sea from satellite data," Geophys. Res. Letters 28, 3963–3966 (2001).

[15] Johannessen, J. A., Kudryavtsev, V., Akimov, D., Eldevik, T., Winther, N., Chapron, B., "On radar imaging of current features: 2. Mesoscale eddy and current front detection," J. Geophys. Research 110 (C7), C07017 (2005).

[16] Font, J., Rousseau, S., Shirasago, B., Garcia-Gorriz, E., Haney, R. L., "Mesoscale variability in the Alboran Sea: Synthetic aperture radar imaging of frontal eddies," J. Geophys. Research 107(C6), 3059 (2002).

[17] Mityagina, M. I.; Lavrova, O. Y.; Uvarov, I. A., "See the Sea: Multi-user information system for investigating processes and phenomena in coastal zones via satellite remotely sensed data, particularly hyperspectral data," Proc. SPIE 9240, 92401C (2014).

[18] Bulatov, M G , Kravtsov, Yu A, Lavrova, O Yu, Litovchenko, K Ts, Mityagina, M I, Raev, M D, Sabinin, K D, Trokhimovskii, Yu G, Churyumov, A N, Shugan, I V., "Physical mechanisms of aerospace radar imaging of the ocean,"Physics-Uspekhi 46 (1), 63-79 (2003).

[19] Alpers W., Chen J. P., Pi Ch.-J., Lin I-I., "On the origin of atmospheric frontal lines off the east coast of Taiwan observed on space-borne synthetic aperture radar images," Mon. Wea. Review 138, 475-496 (2010).

[20] Young, G. S., Johnson, R. H., "Meso- and microscale features of a Colorado cold front," J. Climate Appl. Meteorology 23, 1315–1325 (1984).

[21] Young, G. S., Sikora, T. D., Winstead, N. S., "Use of synthetic aperture radar in fine-scale analysis of synoptic-scale fronts at sea," Weather Forecasting 20, 311-327 (2005).

[22] Schultz, D. M., Blumen, W., [Encyclopedia of Atmospheric Sciences Reference Work], Elsevier, 337-343(2014).

[23] Härtel, C., Carlsson, F., Thunblom, M., "Analysis and direct numerical simulation of the flow at a gravity-current head. Part 2. The lobe-and-cleft instability," Journal of Fluid Mechanics 418, 213-229 (2000).

[24] Weather3.com, "Archive UKMET analysis charts," http://www1.wetter3.de/archiv_ukmet_dt.html (10 July 2018).

[25] Biao, Z., Alpers.W., "The Effect of Rain on Radar Backscattering from the Ocean," https://www.researchgate.net/publication/325170521_The_Effect_of_Rain_on_Radar_Backscattering_from_the_Ocean (Jul 04 2018).

[26] Simpson, J. E., "Gravity currents in the laboratory, atmosphere, and ocean," Annu. Revi. Fluid Mechanics 14(1), 213–234 (1982).

[27] Martin, R. F., "Observations of 250-km-wavelength clear-air eddies and 750-km-wavelength mesocyclones associated with a synoptic-scale midlatitude cyclone," Mon. Wea. Review 124, 1199–1210 (1996).

[28] Hessner, K ., Angelo, R., Peter, B., Alpers, W., "The Rhine Outflow Plume Studied by the Analysis of Synthetic Aperture Radar Data and Numerical Simulations," Journal of Physical Oceanography 31, 3030-3044 (2001).

[29] Li, C., Li, X., Guosheng, Z., Boswell, K., Kimball, M., Shen, D., Lin, J., "Estuarine Plume: A Case Study by Satellite SAR Observations and In Situ Measurements," IEEE Transactions on Geoscience and Remote Sensing (2017).

[30] Zheng, Q., Clemente-Colön, P., Yan, X.-H.,. Liu, W. T, Huang, N. E., "Satellite synthetic aperture radar detection of Delaware Bay plumes: Jet-like feature analysis," J. Geophys. Research 109(C3), C03031 (2004).

[31] Jay, D. A., Zaron, E. D., Pan, J., "Initial expansion of the Columbia river tidal plume: Theory and remote sensing observations," J. Geophys. Research 115(C2), C00B15 (2010).

[32] Matciak, M., Nowacki, J., "The Vistula river discharge front – surface observations," Oceanologia 37(1), 75-88 (1995).

[33] Brandt, P., Romeiser, R., Rubino, A., "On the determination of characteristics of the interior ocean dynamics from radar signatures of oceanic internal solitary waves," J. Geophys. Res. 104, 30039–30046 (1999).

[34] Lavrova O. Yu., Soloviev D. M., Mityagina M. I., Strochkov A. Ya., Bocharova T. Yu., "Revealing the influence of various factors on concentration and spatial distribution of suspended matter based on remote sensing data," Proc. SPIE 9638, 96380D-2 – 96380D-12 (2015).

[35] Askari, F., Geernaert, G. L., Keller, W. C., et al., "Radar imaging of thermal fronts," Int. J. Remote Sens 14, 275-294 (1993).

[36] Weissmann, D. E., Tompson, T. W., Legeckis, R. Modulation of sea surface radar cross section by surface stress: wind speed and temperature effects across the Gulf Stream. J. Geophys. Res. 85(C9), 5032-5042, 1980.

[37] Mityagina M. I., Pungin, V. G., Yakovlev, V. V., "Two-polarization Ku -band radar imagery of sea surface in presence of atmospheric boundary layer motions", Waves in Random Media 8, 111-118 (1998).

[38] Churyumov, A.N., Kravtsov Yu. A, et al., "Resonant and Nonresonant Mechanisms of Forming Space Radar Images of the Ocean", Advances in Space Research 29(1), 11-116 (2002).

[39] Sikora, T. D., Young G. S., Beal, R. C., Monaldo, F. M., Vachon P. W., [Atmosphere-Ocean Interactions Volume 2], WIT Press, Southampton, 83-114 (2006).